Journal of Solid State Electrochemistry
https://doi.org/10.1007/s10008-024-06087-y

ORIGINAL PAPER

Effect of citrate anion incorporation on dielectric properties of anodic oxide grown on Ti-Si alloy

Giada Tranchida[1] · Andrea Zaffora[1] · Francesco Di Franco[1] · Monica Santamaria[1]

Received: 26 June 2024 / Revised: 9 September 2024 / Accepted: 13 September 2024

Abstract

Anodic oxides were galvanostatically grown on sputtered Ti-12at%Si alloy at 5 mA cm^{-2} up to 50 V in phosphoric acid and sodium citrate aqueous electrolytes in order to investigate the effect of anions incorporation (if any) on dielectric properties of the grown oxides. Photoelectrochemical measurements supported the occurrence of incorporation of citrate anions when anodizing is carried out in a citrate-containing solution. Indeed, two different absorption thresholds were estimated due to energy transitions involving localized states in the mobility gap. Differential capacitance measurements showed higher capacitance values for anodic oxide grown in the citrate-containing solution, with a beneficial effect on the dielectric constant. The increased capacitance can be explained considering the synergistic effect of a more favourable anodizing ratio provided by the presence of Si cations from the bare alloy as well as the incorporation of foreign species due to the inward migration of citrate anions from the electrolyte during the anodizing process.

Keywords Anodic oxides · Dielectric constant · Incorporation · Capacitance · Band gap · Electrolytic capacitors

Introduction

High-performance electrolytic capacitors require high-capacitance materials with insulating properties. Currently, commercial electrolytic capacitors are fabricated by employing Al_2O_3 (E_g ranging between 6.2 and 8 eV, $\varepsilon = 9$) or Ta_2O_5 ($\varepsilon = 22$–30) dielectrics (E_g ranging between 3.9 and 4.3 eV). In spite of the high permittivity reported for TiO_2 ($\varepsilon = 24$–53), the use of anodic titanium oxide in micro and nanoelectronics is limited due to the occurrence of crystallization phenomena. Indeed, high voltage anodization of Ti in aqueous electrolyte induces the formation of a significant density of flaws associated with the amorphous-to-crystalline transition during the oxide growth. Ex-situ techniques proved that crystals are formed in the inner part of the growing oxide providing electronic conductive paths for oxygen evolution on crystalline regions [1–3] responsible for the onset of breakdown phenomena with detrimental effect on the efficiency of the device. It is widely known that the amorphous-to-crystalline transition can be hampered by the incorporation of Si due to the outward migration of cations from the bare alloy during the anodizing process [1, 2]. However, the authors experienced a decrease in the permittivity of the anodic film by increasing the silicon content in the alloy.

As widely reported in the literature, a promising strategy to increase the dielectric constant of valve metal oxides used as dielectrics in electronic devices consists of the incorporation of foreign species from the inorganic/organic solution during anodizing [4–10]. As a consequence of the incorporation, the density of states inside the oxide changes due to the formation of localized states in the mobility gap, affecting the electronic properties of the grown oxides.

Several works in the literature are mainly focused on the influence of silicon on the growth and crystallization of anodic oxides grown on Ti-Si alloy [1, 3, 11], as well as on their dielectric constant [2], while the effect of incorporation on electronic properties of anodic films grown on Ti-Si alloys is not investigated. It is noteworthy to mention that although the negative effect of silicon on the dielectric constant of anodic oxides grown on Ti-Si alloy, the latter provides a more favourable anodizing ratio (0.38 nm V^{-1}) [12] compared to that reported for Ti (~2 nm V^{-1}) [13], with a beneficial effect on the capacitance of the anodic film,

✉ Giada Tranchida
giada.tranchida@unipa.it

[1] Applied Electrochemistry Laboratory, Engineering Department, University of Palermo, Viale delle Scienze, Ed. 6, 90128 Palermo, Italy

Published online: 20 September 2024

because of the formation of a thinner layer with equal formation voltage.

In this work, we studied the effect of citrate incorporation on the electronic properties of 50 V anodic oxides grown on Ti-Si sputtering deposited alloys during anodizing in galvanostatic conditions. Photoelectrochemical measurements were carried out in order to get information about the solid-state properties of anodic oxides (e.g., optical band gap and semiconducting or insulating behaviour). Differential capacitance measurements and electrochemical impedance spectroscopy were also performed in order to assess the effect of citrate incorporation on the dielectric properties of the grown oxides.

Experimental

A DC magnetron sputtering method was used for the preparation of Ti-12%Si alloy by co-sputtering 99.5% titanium and 99.999% silicon targets onto glass plates. The 200-nm thick alloy was deposited by using a titanium disc of 100 mm diameter and 6 mm thickness and two square silicon plates with 15 mm sides symmetrically arranged with respect to the sputtered target. In order to get the deposited alloy films of uniform composition and thickness, the holder was rotated around the central axis of the chamber as well as their own axes during sputtering [2, 14]. The composition of the alloy was finally evaluated by Rutherford backscattering spectroscopy (RBS).

The deposited layers were galvanostatically anodized at 5 mA cm^{-2} in 0.1 M phosphoric acid (H_3PO_4) and 1 M sodium citrate ($Na_3C_5H_6O_7$) aqueous solutions at room temperature. The anodic oxides were stabilized for 30 min at a final compliance voltage of 50 V. A two-electrode cell configuration was used consisting of Ti-12%Si alloy and Pt net as anodic and cathodic electrodes, respectively.

Photoelectrochemical (PCS) experiments were performed through a 450-W UV–vis xenon lamp combined with a monochromator (Kratos). The latter allows sample irradiation through a quartz window. The generated photocurrent was separated from the total current in the cell by a mechanical chopper working at 13 Hz coupled with a two-phase lock-in amplifier (EG&G). A more detailed description of the experimental setup used for PCS measurements can be found elsewhere [15, 16].

Photocurrent yield (Q_{ph}) was estimated by taking into account the relative photon flux of the light source at each wavelength (i.e., the efficiency of the lamp-monochromator system).

PCS and impedance measurements were performed in 0.5 M H_2SO_4 by using a three-electrode cell configuration where a silver silver-chloride electrode (0 V vs Ag/AgCl = 0.197 V vs SHE, saturated KCl) was employed as a reference electrode. Electrochemical impedance spectra (EIS) were recorded at different polarizing potentials (i.e., 2 V, 5 V, and 8 V) by scanning a frequency range starting from 10 kHz to 100 mHz while differential capacitance curves were obtained at 100 Hz by sweeping the potential in the cathodic direction starting from 8 V (i.e., a potential value where the oxide does not change) to the equilibrium potential for the hydrogen evolution reaction at the corresponding pH. The amplitude of the superimposed AC signal for both EIS and differential capacitance measurements was fixed at 10 mV. A Parstat 2263 (PAR) coupled with a computer for the acquisition of the experimental data was used for the electrochemical characterization.

Results and discussion

Anodic oxides growth

Figure 1a and b shows the voltage vs time curves for the sputtered Ti-12at%Si during anodizing in phosphoric acid and sodium citrate at 5 mA cm^{-2} to 50 V, respectively.

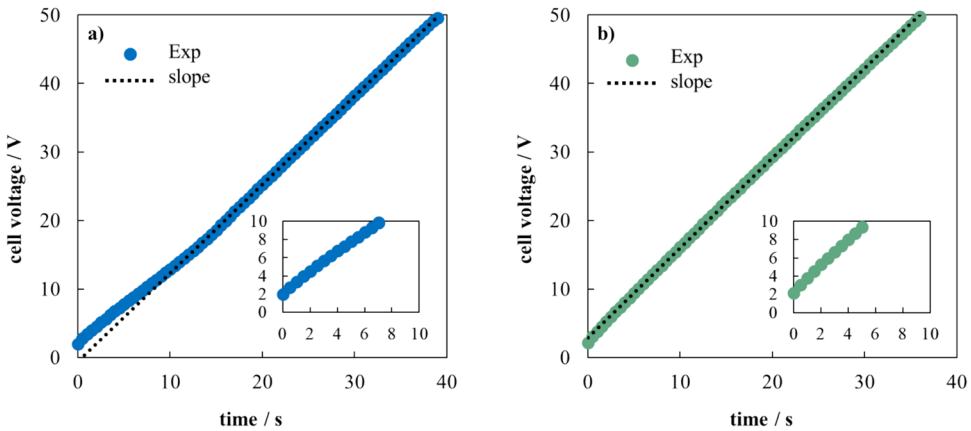

Fig. 1 Voltage-time curves of sputtered Ti-12at%Si alloy during anodizing at 5 mA $cm.^{-2}$ in **a** 0.1 M H_3PO_4 and **b** 1 M $Na_3C_6H_5O_7$

Notably, in both cases, the presence of the air-formed film is evidenced by the initial potential step of about 2 V which is followed by a linear increase of the voltage with time. The slope of the voltage vs time curve slightly changes during the growth, probably due to the ageing of the samples in the laboratory before anodizing treatment that can induce the formation of the precursor of crystalline oxide at the surface of the metal alloys [2, 3]. Then, voltage rises linearly with time up to 50 V as formation voltage, at 1.29 V s^{-1} in the case of anodization in 0.1 M H_3PO_4, and at 1.31 V s^{-1} during anodization in citrate-containing solution. The estimated slope values in the linear growth region are in agreement with those reported for anodic oxides grown on sputtered Ti-Si alloys as a function of silicon content in the bare alloy [2]. This behaviour was rationalized taking into account the formation of amorphous anodic oxide layers without the occurrence of any crystallization phenomena due to the presence of Si in the TiO_2 layer [1–3].

Photoelectrochemical characterization

Photocurrent spectra were recorded in 0.5 M H_2SO_4 at different polarizing potentials in order to estimate the optical band gap ($E_{g,opt}$) of anodic oxides grown in incorporating electrolytes. Photocurrent vs irradiating wavelength curves recorded at 8 V vs Ag/AgCl for the films grown in phosphate and citrate-containing solutions are displayed in Fig. 2a and b, respectively.

The latter allows to estimate $E_{g,opt}$ for all the investigated films by considering the proportionality between Q_{ph} and the light absorption coefficient for a photon energy in the vicinity of the band gap, as follows:

$$(Q_{ph} \cdot h\nu)^n \propto (h\nu - E_{g,opt}) \quad (1)$$

where $h\nu$ is the photon energy. Assuming 0.5 for the exponent n for non-direct optical transition for amorphous materials, it is possible to estimate the value of $E_{g,opt}$ by extrapolating to zero $(Q_{ph} \bullet h\nu)^{0.5}$ vs hν plot, as shown in the inset of Fig. 2.

According to Eq. (1), for anodic oxide grown on Ti-12 at%Si alloy in 0.1 M phosphoric acid, an $E_{g,opt}$ of 3.52 eV was estimated higher than the typical optical band gap values of the crystalline TiO_2, namely, anatase ($E_g = 3.2$ eV) and rutile ($E_g = 3.05$ eV). As widely explained in previous works [11, 17], this difference with the crystalline counterparts can be attributed to the amorphous nature of the oxides due to a distribution of localized states near the conduction and valence band edges. This finding is also in agreement with previous experimental results reported for 40 V anodic oxides grown in the same anodizing electrolyte on Ti-6 at%Si alloy [11]. For the latter, an optical band gap value of 3.40 eV was estimated, higher than that obtained in the same

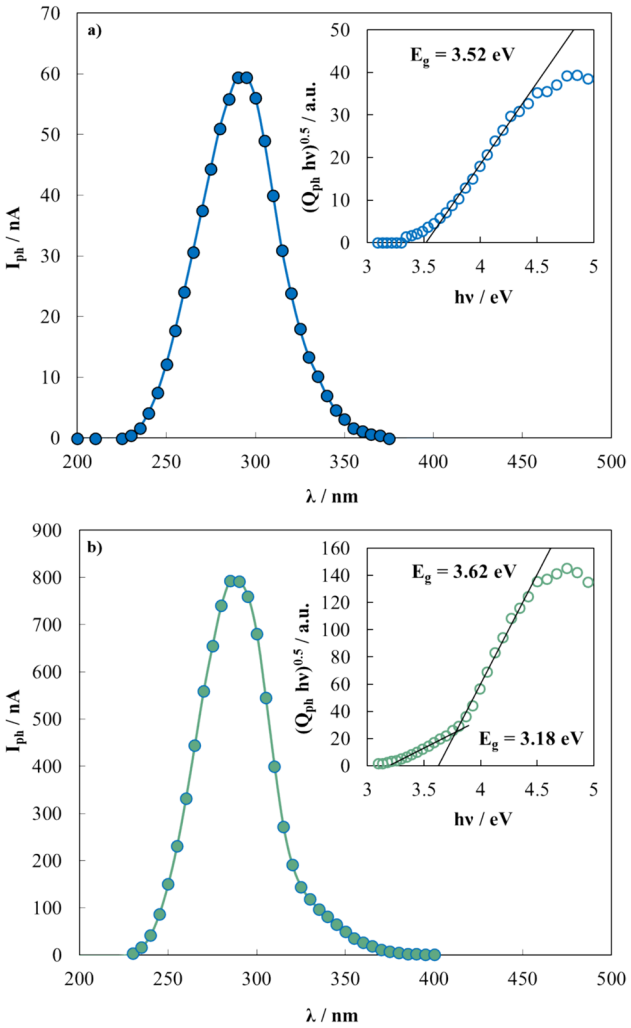

Fig. 2 **a** Photocurrent vs irradiating wavelength relating to anodic film grown at 5 mA cm^{-2} to $U_F = 50$ V on Ti-12at%Si alloy in **a** 0.1 M H_3PO_4 and **b** 1 M $Na_3C_6H_5O_7$ recorded in 0.5 M H_2SO_4 at $U_E = 8$ V vs Ag/AgCl. Inset, band gap estimation by assuming a non-direct optical transition

growth condition for pure Ti (i.e., $E_{g,opt} = 3.3$ eV), confirming the beneficial effect of Si in hindering the amorphous-to-crystalline transition.

For anodic oxides grown in 1 M sodium citrate solution, two different absorption threshold values were estimated (see Fig. 2b), where the higher ($E_{g,opt} = 3.62$ eV) is associated with energy transition between the conduction and the valence band edges while the lower ($E_{LS} = 3.18$ eV) involves energy transitions associated to the presence of localized states in the mobility gap (i.e., localized-extended states optical transitions). Indeed, the presence of energy transitions other than band-to-band transitions is usually attributed to the incorporation of negatively charged species from the electrolyte (in this case citrate anions) inside the film, as already evidenced during anodization of valve metal and valve metal

alloy in incorporating aqueous electrolytes [4, 8, 15, 18, 19]. In Table 1, optical band gap values obtained by following Eq. (1) for all the investigated anodic oxides are reported.

The presence of two different absorption thresholds in this case suggests the formation of a double-layered structure consisting of inner (i.e., citrate-free) and outer (i.e., citrate-containing) layers with different optical properties in terms of mobility of photocarriers and optical band gap values. This assumption is also supported by the fact that usually foreign species are incorporated from the electrolyte only in an outer layer during the anodizing process as reported in the literature [14, 15, 19–21]

The photoelectrochemical behaviour of the layered structure can be studied by considering the dependence of the total photocurrent (namely, I_{ph} provided by both the inner and outer layer) on the energy of the incident light, the thickness of the anodic oxide (d), and the applied electric field (E) [8, 15]. Basically, the collected photocurrent can be expressed as a generation contribution G, accounting for the efficiency generation of the photocarriers (η_g), expressed as:

$$G = \eta_g\left[1 - \exp\left(-\alpha D\right)\right] \tag{2}$$

where α is the absorption coefficient times the transport term T:

$$T = \frac{\mu\tau F}{D}\left[1 - \exp\left(-\frac{D}{\mu\tau F}\right)\right] \tag{3}$$

that is strictly related to the mobility (μ) and lifetime (τ) of photogenerated carriers, respectively for electrons and holes, as follows:

$$\mu\tau = \mu_e\tau_e + \mu_h\tau_h \tag{4}$$

Therefore, for a double-layered structure, the photocurrent can be written as:

$$I_{ph} = I_{ph,out} + I_{ph,inn} \tag{5}$$

Table 1 Band gap values estimated for anodic oxides grown on Ti-12at%Si alloy at 5 mA cm^{-2} to 50 V in 0.1 M H_3PO_4 and 1 M $Na_3C_6H_5O_7$

	$E_{g,opt}$/eV	E_{LS}/eV
0.1 M H_3PO_4		
5 V vs Ag/AgCl	3.47	N.D
8 V vs Ag/AgCl	3.52	N.D
1 M $Na_3C_6H_5O_7$		
5 V vs Ag/AgCl	3.63	3.18
8 V vs Ag/AgCl	3.62	3.18

where $I_{ph,out}$ is the contribution provided from the outer phase (i.e., citrate-containing phase), while $I_{ph,inn}$ is that coming from the inner layer (i.e., citrate-free layer).

Moreover, by considering the photocurrent yield, defined as:

$$Q = \frac{I_{ph}}{e\varphi_0(1-R)} \tag{6}$$

where φ_0 the photon flux impinging the oxide surface and R the reflection at the metal/oxide/electrolyte interface, Eq. (5) can be written as:

$$I_{ph} = e\varphi_0(1-R)\left[T_{out}G_{out} + exp\left(-\alpha_{out}d_{out}\right) \times T_{inn}G_{inn}\right] \tag{7}$$

where d_{out} is the thickness of the outer layer.

Finally, taking into account the dependence of the absorption coefficient from the photon energy:

$$\alpha = A\frac{\left(h\nu - E_g\right)^n}{h\nu} \tag{8}$$

where hν, E_g, and n keep the aforementioned meaning, and A is a constant whose value depends on the material, and combining Eq. (8) with Eqs. (6) and (5), for non-direct optical transitions, the following equation holds:

$$(Q \times h\nu)^{1/2} = \left[\left(T_{out}G_{out} + e^{-\alpha_{out}d_{out}} \times T_{inn}G_{inn}\right)h\nu\right]^{1/2} \tag{9}$$

considering $\Phi_0 e^{-\alpha_{out}d_{out}}$ as the photon flux incident to the inner layer surface and the generation efficiency equal 1 at a high anodic potential. Equation (9) was then used for the interpolation of photocurrent spectra allowing a more affordable estimation of the band gap values of both inner and outer layer. Notably, d_{out} equal to ~ 60% of the total thickness was assumed for the best fitting procedure, in agreement with the incorporation of foreign species from the electrolyte during the anodizing process in the outer layer of the growing oxide [9, 19]. The theoretical fitting obtained according to Eq. (9) for anodic film grown in citrate solution is consistent with the experimental data, as shown in Fig. 3.

In Table 2 fitting parameters are listed.

Notably, the reported mobility values for the citrate-free layer (i.e., inner layer) are in agreement with the values reported in previous works ($\mu\tau_{inn}$~10^{-13} cm^2 V^{-1}) [11], while an order of magnitude lower mobility was extrapolated for the outer phase. This finding is in agreement with the lower mobility of the photogenerated carriers in the citrate-containing phase due to the presence of localized states as a consequence of the inward migration of citrate anions during the anodizing process.

In Fig. 4, we have reported the total circulating current with (on) and without (off) irradiation in the oxides

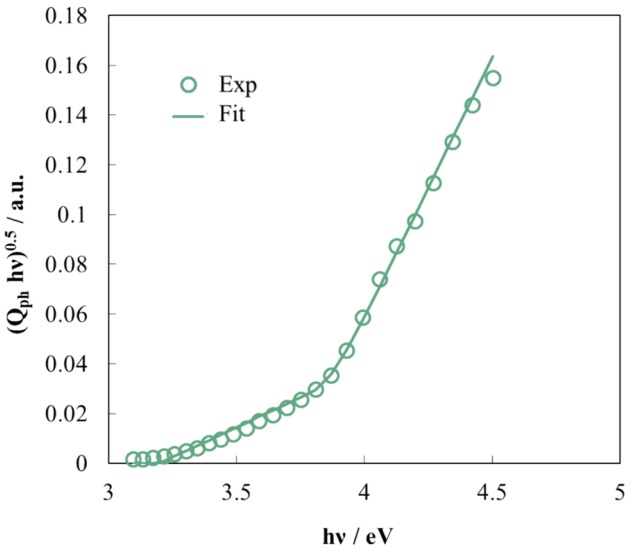

Fig. 3 Theoretical fitting (green continuous line) in agreement with Eq. (9) of the photocurrent spectrum recorded in 0.5 M H_2SO_4 at $U_E = 8$ V vs Ag/AgCl for the anodic oxide grown in citrate containing solution at 5 mA cm^{-2} to 50 V

Table 2 Fitting parameters of photocurrent spectrum recorded at $U_E = 8$ V vs Ag/AgCl in 0.5 M H_2SO_4 for anodic film galvanostatically grown on Ti-12at%Si to 50 V at 5 mA cm^{-2} in 1 M $Na_3C_6H_5O_7$ according to Eq. (9)

	$(\mu\tau)_{\text{citrate free}}$ [$cm^2\ V^{-1}$]	$E_{g,\text{ citrate free}}$ [eV]	$(\mu\tau)_{\text{citrate containing}}$ [$cm^2\ V^{-1}$]	$E_{g,\text{ citrate containing}}$ [eV]
Ti-12at%Si anodized to 50 V	1.50×10^{-13}	3.8	2.00×10^{-14}	3.2

recorded in 0.5 M H_2SO_4 at 2 V vs Ag/AgCl for different irradiating wavelengths.

The recorded photocurrent is anodic for both anodic oxides, as expected for n-type semiconductors. Notably, in the case of anodic film grown in phosphoric acid, anodic spikes of the current after irradiation were recorded, suggesting that photogenerated carriers are involved in recombination phenomena. Conversely, in the case of anodic film grown in a citrate-containing solution, the circulating current reaches a stationary value soon after sample irradiation (on). Notably, for the latter, the recorded photocurrent is significantly higher than that obtained for anodic oxide grown in a phosphoric acid solution.

It is important to underlying that the theoretical fitting for citrate-containing oxide provided lower mobility of the photocarriers (i.e., lower μτ value than that estimated for citrate-free oxide) that seems to be in contrast with the very high measured photocurrent, as displayed in Fig. 2. However, as stated above, I_{ph} depends on both generation and transport efficiencies, as predicted by Eq. (9). Therefore, the presence of anodic spikes in the case of anodic oxide grown in phosphoric acid solution (see Fig. 4a) indicates significant geminate recombination of photocarriers [15].

In Fig. 5, normalized photocurrent versus potential curves (i.e., photocharacteristics) relating to anodic films grown on Ti-12at%Si alloy at 5 mA cm^{-2} at different constant irradiating wavelengths are reported.

As expected for a n-type SC, the photocurrent decreases by decreasing the polarizing potential, in both cases. In addition, the shape of the photocharacteristic provides information about the less crystalline/amorphous nature of the grown oxides as well as the occurrence of recombination phenomena [4, 11]. Indeed, according to the Gartner–Butler model valid for a crystalline SC/electrolyte junction, no influence of the irradiating wavelength on the shape of the I_{ph} vs U_E curves and a linear dependence of I_{ph}^2 on the electrode potential are predicted. However, the best fitting procedure of the photocharacteristics is according to the following power law:

$$I_{ph}^{\ n} \propto U_E \tag{10}$$

valid for amorphous materials, provided n is significantly lower than 2 (i.e., supralinear behaviour), suggesting the formation of amorphous oxides with a lower mobility of the photogenerated carriers in the localized states. In Table 3, the values of the exponent n estimated from the best fitting procedure according to Eq. (10) are reported.

It is important to mention that n is also significantly lower than the values reported for Ti-6at%Si alloy [11], probably due to the higher amount of Si from the bare alloy. Notably, in the case of anodic film grown in citrate-containing solution ($n \sim 0.5$), the reported values are slightly higher than those obtained for anodic oxide grown in phosphoric acid ($n \sim 0.4$) suggesting the formation of a slightly less amorphous oxide. This finding matches with the significantly lower photocurrent recorded in the case of anodic film grown in phosphoric acid solution.

Electrochemical characterization

Figure 6a and b displays the modified Bode representation of the electrochemical impedance spectra (EIS) related to the oxide films grown in phosphoric acid and sodium citrate, respectively, recorded in 0.5 M H_2SO_4 at 8 V vs Ag/AgCl.

The electrical equivalent circuit (ECC) reported in the inset of Fig. 6 was used in order to properly model the electrochemical behaviour of the metal/anodic oxide/electrolyte interface for the investigated films. The ECC used for the best-fitting procedure accounts for a double-layered structure of the anodic oxide due to the incorporation of Si from the bare alloy during the anodization process [2, 11]. The latter consists of two

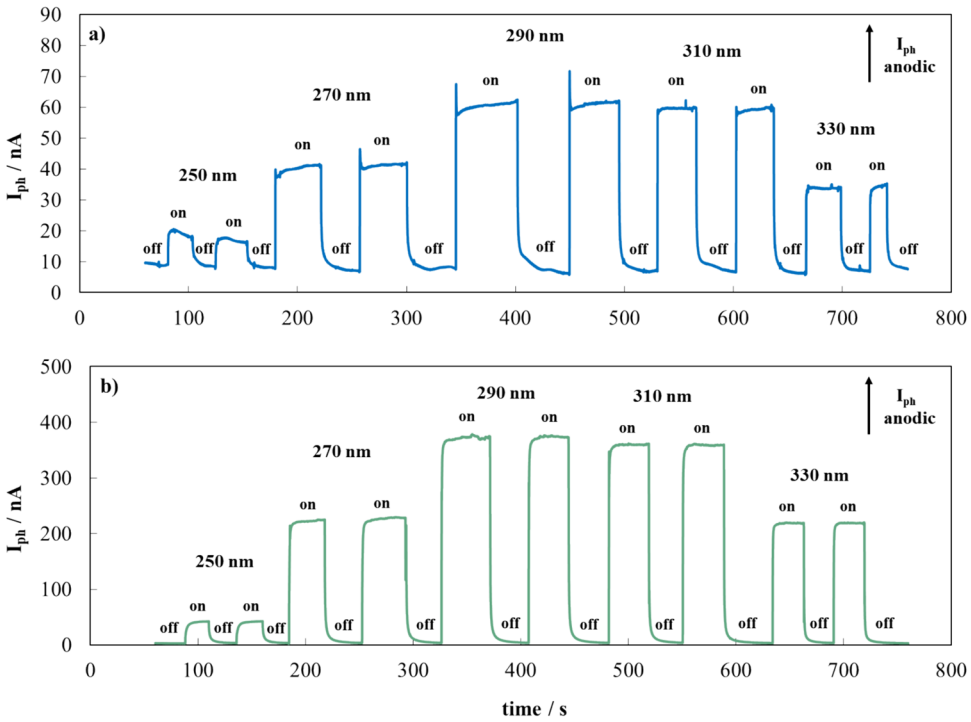

Fig. 4 Current transients recorded at 2 V vs Ag/AgCl at different irradiating wavelengths in 0.5 M H_2SO_4 for anodic oxide grown on Ti-12at%Si alloy in **a** 0.1 M H_3PO_4 and **b** 1 M $Na_3C_6H_5O_7$

parallel (RQ), where Q is the constant phase element accounting for the non-ideal capacitance behaviour of the interface under investigation, and R is the resistance of the considered anodic layer (with and without Si), in series with the electrolyte resistance, R_{el}. The fitting parameters of the impedance spectra for all the investigated samples recorded at different applied electrode potentials (i.e., 2, 5, and 8 V vs Ag/AgCl) are listed in Table 4. The validity of the EIS data was verified by the application of Kramers–Kronig transformations.

However, it is noteworthy to mention that the electrochemical impedance spectra of Fig. 6a and b are very similar to each other, suggesting that the ECC used for the best fitting procedure likely models the double-layered structure due to Si incorporation from the bare alloy.

Therefore, differential capacitance curves were recorded in order to gain more insight about the dielectric properties of the grown oxides. According to modern electrolytic capacitors standardized measurement method [22], the capacitance of the anodic oxides was investigated at 100 Hz. Capacitance vs potential curves recorded in 0.5 M H_2SO_4 at 50 mV s^{-1} by sweeping the potential from 8 V to the equilibrium potential for the hydrogen evolution reaction at the corresponding pH are displayed in Fig. 7.

Notably, for both anodic oxides, the recorded capacitance increases when the electrode potential decreases, as expected for n-SC. Moreover, the estimated capacitance reveals the formation of a more polarizable anodic oxide approaching the flat band potential when it is grown in citrate incorporating solution, in agreement with a large extent of defects in the mobility gap due to the incorporation of citrate anions. Conversely, in the case of anodic oxide grown in phosphoric acid, the recorded capacitance slightly changes with the applied potential in agreement with the formation of a more insulating material. Finally, for the anodic oxide grown in sodium citrate a capacitance value of ~ 4.2 μF cm^{-2} was measured at high band-bending. This finding is also supported by fitting parameters (see Table 4).

The effect of the incorporation of foreign species from the electrolyte during the anodizing process on the electronic properties of anodic oxides grown on sputter-deposited Ti-12at%Si alloy can be assessed by the estimation of the dielectric constant. In particular, by the knowledge of the capacitance evaluated at 8 V vs Ag/AgCl (namely, high band bending condition), it is possible to obtain the ε/d ratio for both anodic oxides. Considering that for anodic oxides grown on sputter-deposited Ti-Si alloys an anodic ratio of 1.94 nm V^{-1} can be extrapolated [2, 11], a dielectric constant value of about 37 was obtained for anodic oxide grown after anodization at 5 mA cm^{-2} in phosphoric acid solution, in agreement with the values reported in the literature [2]. On the other hand, a dielectric constant of ~ 46 was estimated in the case of anodic film grown in 1 M sodium citrate, very close to that reported for anodic TiO_2 grown on pure titanium (i.e., ~ 50). This finding suggests that the decrease in the dielectric constant due to the incorporation of silicon from the alloy during anodic oxide growth could be compensated by performing anodization in citrate anion-containing solutions. Despite the

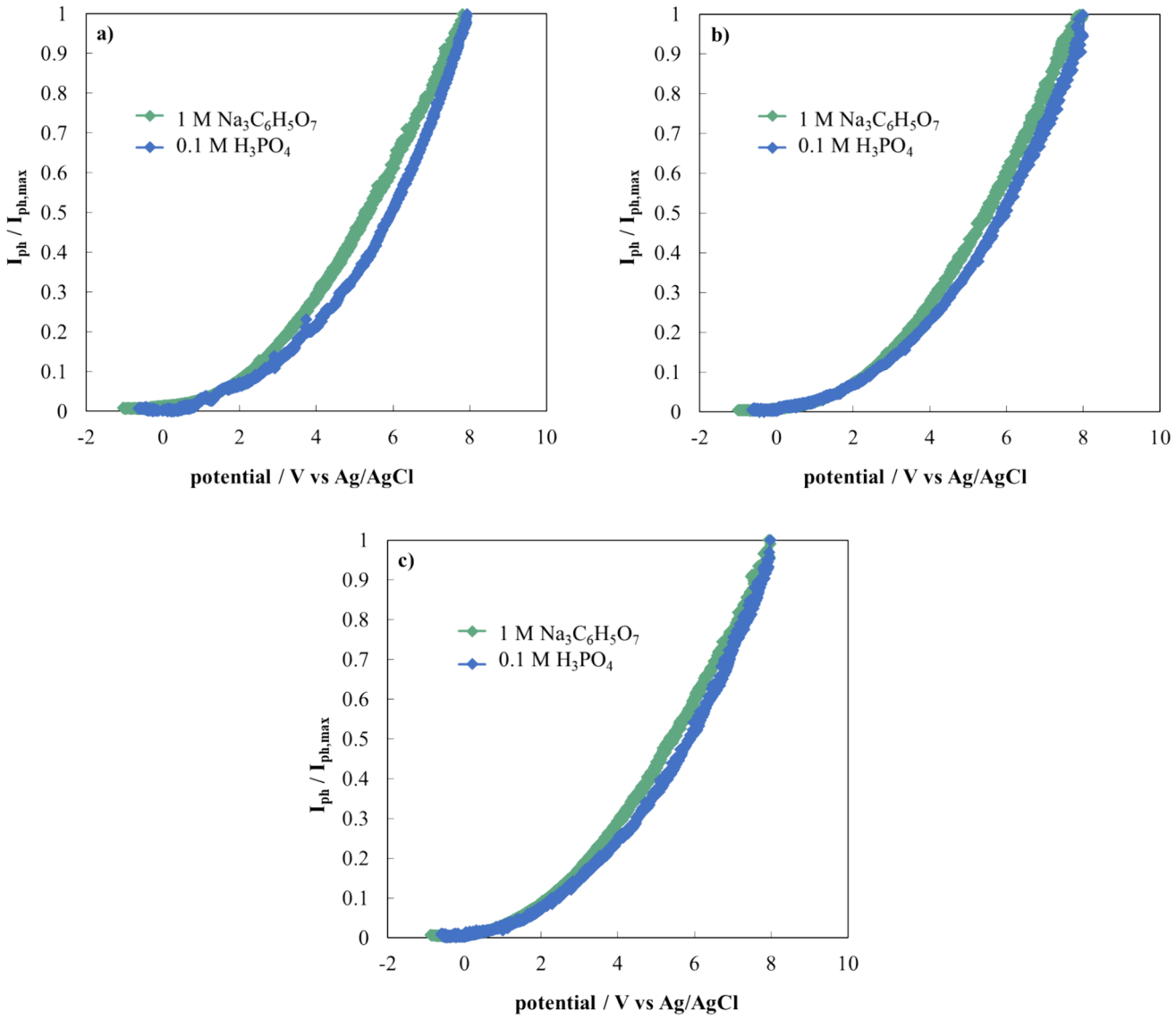

Fig. 5 Normalized photocurrent vs potential curves related to anodic films grown at 5 mA cm^{-2} to $U_F = 50$ V on Ti-12at%Si alloy in 0.5 M H_2SO_4 at 10 mV s^{-1} at **a** 270 nm, **b** 290 nm, and **c** 310 nm

Table 3 Exponent *n* estimated from the best fitting of the photocurrent vs potential curves related to anodic films grown on Ti-12at%Si according to Eq. (10)

	λ/nm	n
Anodic oxide grown in phosphoric acid	270	0.35
	290	0.40
	310	0.45
Anodic oxide grown in sodium citrate	270	0.50
	290	0.50
	310	0.55

unfavourable anodizing ratio of titanium, the boosting on the dielectric constant value allows the growth of dielectric materials with high specific capacitance.

The increased permittivity of the citrate-containing oxide can be explained considering both the higher polarizability of $C_6H_5O_7^{3-}$ with respect to the O^{2-} and the local structure disorder due to the substitutional citrate anions, as already reported for N-doped anodic oxides grown on Ta-Nb sputtering-deposited alloys [8, 23].

Conclusion

Anodization of sputter-deposited Ti-12at%Si alloy in phosphoric acid and sodium citrate solution at 5 mA cm^{-2} and 50 V was performed with the aim to grow high permittivity

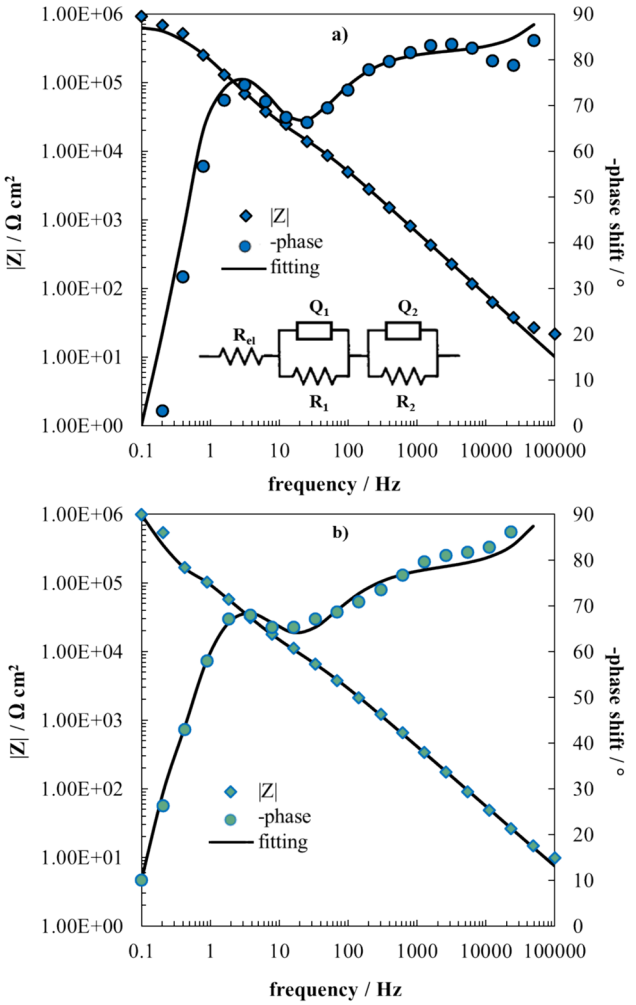

Fig. 6 Modified Bode representation of the EIS spectra recorded at 8 V vs Ag/AgCl in 0.5 M H_2SO_4 related to anodic films grown at 5 mA cm^{-2} to 50 V on Ti-12at%Si alloy in **a** 0.1 M H_3PO_4 and **b** 1 M $Na_3C_6H_5O_7$. $R_{el} = 40\ \Omega\ cm^2$

materials to be employed as dielectrics in electrolytic capacitors.

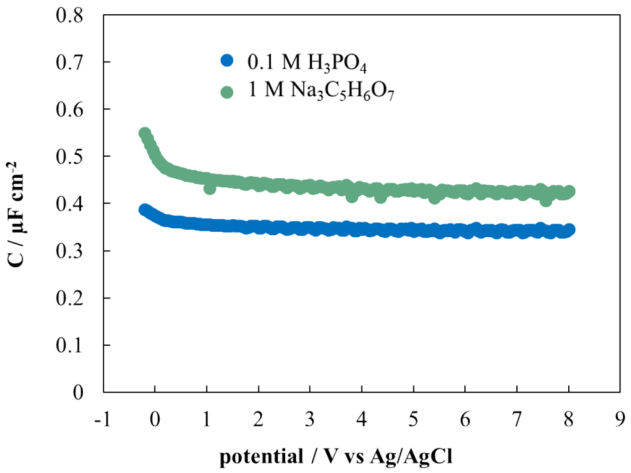

Fig. 7 Differential capacitance curves relating to anodic films grown at 5 mA cm^{-2} to $U_F = 50$ V on Ti-12at%Si alloy in 0.1 M H_3PO_4 and 1 M $Na_3C_6H_5O_7$ recorded in 0.5 M H_2SO_4 at 50 mV s^{-1} and 100 Hz

Photoelectrochemical measurements revealed the formation of anodic oxides with a band gap value higher than those reported for the crystalline TiO_2, confirming the worthwhile effect of silicon in hampering amorphous-to-crystalline transition during anodization at high growth potential in both solutions. Moreover, a red shift in the optical absorption threshold was evidenced in the case of anodic oxides grown in sodium citrate ($E_g = 3.18$ eV), due to the formation of localized states in the band gap, related to the occurrence of citrate anions incorporation during anodizing process.

Photocurrent vs potential curves revealed the formation of amorphous n-type semiconductors, independently of the employed solution, as supported by the best fitting procedure of the photocurrent vs potential curves.

Electrochemical impedance spectroscopy measurements confirmed the double-layered structure of the layers due to the incorporation of silicon from the bare alloy, while differential capacitance measurements showed that the highest

Table 4 Fitting parameters of the EIS spectra recorded for anodic oxides grown in phosphoric acid and sodium citrate electrolyte by using the ECC reported in the inset of Fig. 5

	R_1 (Ω cm^2)	Q_1 (S $s^{\alpha} cm^{-2}$)	α_1	R_2 (Ω cm^2)	Q_2 (S $s^{\alpha} cm^{-2}$)	α_2	χ^2
0.1 M H_3PO_4							
2 V vs Ag/AgCl	1.00×10^6	8.78×10^{-7}	0.97	1.39×10^4	1.06×10^{-6}	0.88	4.38×10^{-3}
5 V vs Ag/AgCl	6.09×10^5	7.57×10^{-7}	1	1.40×10^4	9.67×10^{-7}	0.88	7.31×10^{-3}
8 V vs Ag/AgCl	6.40×10^5	7.34×10^{-7}	1	1.11×10^4	1.09×10^{-6}	0.87	1.11×10^{-2}
1 M $Na_3C_6H_5O_7$							
2 V vs Ag/AgCl	3.49×10^6	1.76×10^{-6}	0.93	6960	1.50×10^{-6}	0.85	4.48×10^{-3}
5 V vs Ag/AgCl	7.82×10^5	1.42×10^{-6}	0.99	7976	2.31×10^{-6}	0.83	1.51×10^{-2}
8 V vs Ag/AgCl	2.56×10^5	1.76×10^{-6}	0.93	5662	2.53×10^{-6}	0.84	1.97×10^{-3}

$R_{el} = 40\ \Omega\ cm^2$

capacitance value was obtained for anodic film grown in citrate-containing solution, with an increase of ~ 24% with respect to that estimated for oxides grown in phosphoric acid aqueous electrolyte. The improvement in the dielectric constant evidenced by capacitance measurements suggests that anodization in citrate solution can be considered a promising strategy for the fabrication of titanium-based capacitors.

Acknowledgements The authors gratefully acknowledge H. Habazaki (Faculty of Engineering, Hokkaido University, Japan) for providing sputtering-deposited samples.

Author contributions Material preparation and data collection: Giada Tranchida; conceptualization: Andrea Zaffora, Francesco di Franco, and Monica Santamaria; methodology: Andrea Zaffora, Francesco di Franco, and Monica Santamaria; formal analysis and investigation: Giada Tranchida, Andrea Zaffora, and Francesco di Franco; writing—original draft preparation: Giada Tranchida; writing—review and editing: Andrea Zaffora, Francesco di Franco, and Monica Santamaria; funding acquisition: Monica Santamaria; resources: Monica Santamaria; supervision: Monica Santamaria. All authors read and approved the final manuscript.

Funding Open access funding provided by Università degli Studi di Palermo within the CRUI-CARE Agreement.

Data availability The datasets generated during and/or analysed during the current study are available from the corresponding author upon reasonable request.

Declarations

Conflict of interest The authors declare no competing interests.

References

1. Habazaki H, Shimizu K, Nagata S et al (2002) Ionic transport in amorphous anodic titania stabilised by incorporation of silicon species. Corros Sci 44:1047–1055
2. Tanvir MT, Fushimi K, Shimizu K et al (2007) Influence of silicon on the growth of barrier-type anodic films on titanium. Electrochim Acta 52:6834–6840. https://doi.org/10.1016/j.electacta.2007.04.113
3. Habazaki H, Uozumi M, Konno H et al (2003) Crystallization of anodic titania on titanium and its alloys. Corros Sci 45:2063–2073. https://doi.org/10.1016/S0010-938X(03)00040-4
4. Zaffora A, Di Franco F, Di Quarto F, Santamaria M (2020) Optimization of anodizing process of tantalum for Ta2O5-based capacitors. J Solid State Electrochem 24:2953–2962. https://doi.org/10.1007/s10008-020-04704-0
5. Tranchida G, Zaffora A, Di Franco F, Santamaria M (2022) The effect of anodizing bath composition on the electronic properties of anodic Ta-Nb mixed oxides. Nanomaterials. https://doi.org/10.3390/nano12244439
6. Zaffora A, Santamaria M, Di Franco F et al (2016) Photoelectrochemical evidence of nitrogen incorporation during anodizing sputtering-deposited Al-Ta alloys. Phys Chem Chem Phys 18:351–360. https://doi.org/10.1039/c5cp04347f
7. Kim Y-H, Uosaki K (2013) Preparation of tantalum anodic oxide film in citric acid solution - evidence and effects of citrate anion incorporation. J Electrochem Sci Technol 4:163–170. https://doi.org/10.5229/jecst.2013.4.4.163
8. Di Franco F, Zaffora A, Santamaria M (2018) Band gap narrowing and dielectric constant enhancement of (NbxTa(1–x))2O5 by electrochemical nitrogen doping. Electrochim Acta 265:326–335. https://doi.org/10.1016/j.electacta.2018.01.182
9. Ono S, Kuramochi K, Asoh H (2009) Effects of electrolyte pH and temperature on dielectric properties of anodic oxide films formed on niobium. Corros Sci 51:1513–1518. https://doi.org/10.1016/j.corsci.2008.11.027
10. Sato Y, Asoh H, Ono S (2013) Effects of electrolyte species and their combination on film structures and dielectric properties of crystalline anodic alumina films formed by two-step anodization. Mater Trans 54:1993–1999. https://doi.org/10.2320/matertrans.L-M2013826
11. Di Quarto F, Di Franco F, Monarca C et al (2013) Photoelectrochemical characterization of amorphous anodic films on Ti-6at.%Si. Electrochim Acta 110:517–525. https://doi.org/10.1016/j.electacta.2013.01.120
12. Schmidt PF, Michel W (1957) Anodic formation of oxide films on silicon. J Electrochem Soc 104:230–236. https://doi.org/10.1149/1.2428542
13. Lohrengel MM (1993) A review journal. Thin anodic oxide layers on aluminium and other valve metals: high field regime. Mat Sci Eng Rll 11:243–294. https://doi.org/10.1016/0927-796X(93)90005-N
14. Habazaki H, Fushimi K, Shimizu K et al (2007) Fast migration of fluoride ions in growing anodic titanium oxide. Electrochem commun 9:1222–1227. https://doi.org/10.1016/j.elecom.2006.12.023
15. Zaffora A, Santamaria M, Di FF et al (2016) Photoelectrochemical evidence of inhomogeneous composition at nm length scale of anodic films on valve metals alloys. Electrochim Acta 201:333–339. https://doi.org/10.1016/j.electacta.2015.12.157
16. Zaffora A, Di Quarto F, Kura C et al (2018) Electrochemical oxidation of Hf–Nb alloys as a valuable route to prepare mixed oxides of tailored dielectric properties. Adv Electron Mater. https://doi.org/10.1002/aelm.201800006
17. Di Quarto F, Piazza S, Santamaria M (2009) Physicochemical characterization of passive films and corrosion layers by differential admittance and photocurrent spectroscopy. In: Pyun S-I, Lee J-W (eds) Modern aspect of electrochemistry: progress in corrosion science and engineering I. Springer, New York, pp 231–316. https://doi.org/10.1007/978-0-387-92263-8
18. Di Franco F, Santamaria M, Di Quarto F et al (2012) The influence of nitrogen incorporation on the optical properties of anodic Ta2O5. Electrochim Acta 59:382–386. https://doi.org/10.1016/j.electacta.2011.10.086
19. Shimizu K, Habazaki H, Skeldon P et al (2001) Migration of oxalate ions in anodic alumina. Electrochim Acta 46:4379–4382
20. Habazaki H, Teraoka M, Aoki Y et al (2010) Formation of porous anodic titanium oxide films in hot phosphate/glycerol electrolyte. Electrochim Acta 55:3939–3943. https://doi.org/10.1016/j.electacta.2010.02.036

21. Lu Q, Skeldon P, Thompson GE et al (2004) Transport numbers of metal and oxygen species in anodic tantala. Corros Sci 46:2817–2824. https://doi.org/10.1016/j.corsci.2004.03.021
22. TDK (2022) Aluminum electrolytic capacitors general technical information. https://www.tdk-electronics.tdk.com/download/185386/e724fb43668a157bc547c65b0cff75f8/pdfgeneraltechnicalinformation.pdf
23. Han HD, Kim JM, Il KY (2017) Effect of partial nitridation on the dielectric constant of A5Ta4O15 (A=Sr, Ba). Ceram Int 43:766–770. https://doi.org/10.1016/j.ceramint.2016.10.007